American Mineralogist, Volume 72, pages 137–147, 1987

An unusual pyroxene, melilite, and iron oxide mineral assemblage in a coal-fire buchite from Buffalo, Wyoming

Franklin F. Foit, Jr.
Department of Geology, Washington State University, Pullman, Washington 99164, U.S.A.

Robert L. Hooper
Department of Geology, University of Wisconsin–Eau Claire, Eau Claire, Wisconsin 54701, U.S.A.

Philip E. Rosenberg
Department of Geology, Washington State University, Pullman, Washington 99164, U.S.A.

Abstract

Near-surface combustion of the Healy coal seam near Buffalo, Wyoming, baked and partially fused a 20-m-thick overlying sequence of sandstone, siltstone, and shale producing a multi-colored vesicular rock resembling slag (buchite). This coal-fire buchite is highly heterogeneous and consists largely of clinopyroxenes, melilites, and oxides, with minor glass. The pyroxenes are unusually rich in Al and Fe^{3+}, and the Fe^{3+}-rich melilites and oxides have chemical compositions heretofore unreported in nature.

Clinopyroxene compositions straddle the diopside (Di)–ferri-aluminum Tschermaks (FATs) join in the system Di-CaTs ($CaAl_2SiO_6$)–FTs ($CaFe^{3+}_2SiO_6$) and range from $Di_{80}FTs_{12}CaTs_8$ to $Di_9FTs_{52}CaTs_{39}$. Compositions approaching the FATs endmember have a maximum tetrahedral Fe^{3+} content of 0.17 atoms per formula unit (8.5% tetrahedral occupancy). In the melilites, extensive coupled substitution of the type $Fe^{3+} + Al^{3+} = Si^{4+} + R^{2+}$ produces compositional variation away from the gehlenite-ferrigehlenite join, $R^{2+}_2(Al_2SiO_7)$-$R^{2+}_2(Fe^{3+}_2SiO_7)$, and toward the hypothetical endmember $R^{2+}R^{3+}(R^{3+}_3O_7)$. The substitution of Fe^{3+} and Al for Si and R^{2+} appears to involve both the four and the eight-coordinated sites and results in an Fe^{3+} content higher than in endmember ferrigehlenite. Both hematite and magnesioferrite show extensive $Al \rightarrow Fe^{3+}$ substitution resulting in a solid-solution series from magnesioferrite, $Fe^{3+}(Fe^{3+},Mg)O_4$, along the spinel-magnesioferrite join to $Sp_{80}Mf_{20}$ and along the magnesioferrite-hematite join to $Mf_{60}Hm_{40}$. Most compositions lie in the Al-rich field and have formulas that are slightly cation deficient. The chemical data suggest the presence of a miscibility gap between Sp_{100} and $Sp_{80}Mf_{20}$ and a solvus dome between hematite and magnesioferrite solid solutions.

Introduction

Coal-fire buchites (partially fused rocks) produced by the in situ, near-surface natural combustion of coal seams are common geologic features in the western United States. Despite their conspicuous presence and utilization as a source of road metal, little is known of their mineralogy. A buchite that crops out east of Buffalo, Wyoming (Fig. 1), contains an unusual silicate and oxide mineral assemblage, which is the subject of this paper.

Geologic setting

Many of the buttes and divides east of Buffalo, Wyoming, are capped with clinker produced by the near-surface combustion of the Walters and Healy coal seams contained in the Wasatch Formation (Dobrovolny, 1981). The buchite sample examined in this study was taken from a clinker outcrop exposed along Interstate 90 approximately 4 km east of Buffalo, Wyoming. Combustion of the Healy seam, which locally has a thickness of approximately 5 m (Mapel, 1959), thermally altered a 20-m-thick sequence of shales, siltstones, and sandstones. The zone of alteration is predominantly red owing to the abundance of finely disseminated iron oxides, but in several places the overlying strata underwent partial fusion, resulting in a black vesicular rock assembling slag (buchite). The largely greenish-black buchite is in direct contact with a reddish-brown siliceous shale that shows no evidence of partial fusion. The protolith for the buchite was probably a calcareous siltstone or shale, both of which stratigraphically overlie the Healy seam.

Methods of analysis

The buchite sample chosen for detailed examination is mottled in hues of orange-red, pale yellow-green, and black and resembles a highly vesiculated smelter slag. The sample was sectioned across the macroscopically colorful zones, and coverless thin sections were prepared for petrographic and electron-microprobe analysis. Small fragments of mineralogically interesting zones were ground to 200 mesh and separated, using magnetic

0003–004X/87/0102–0137$02.00

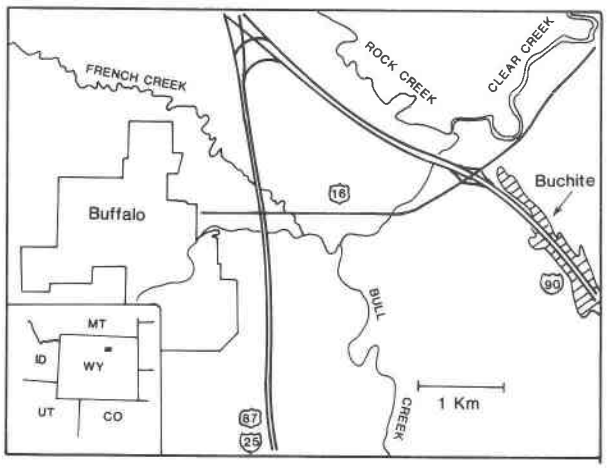

Fig. 1. Map showing the location of the buchite along Interstate 90 near Buffalo, Wyoming.

Table 1. Chemical analyses of the Buffalo, Wyoming, coal-fire buchite

Oxide	Bulk chemistry* (wt%)	Glass chemistry† (wt%)
SiO_2	47.24	54.59
Al_2O_3	20.46	22.80
K_2O	1.32	10.82
Na_2O	1.36	6.11
CaO	9.80	0.64
MgO	2.19	0.25
Fe_2O_3**	14.87	3.41
TiO_2	0.80	0.55
MnO	0.12	0.04
P_2O_5	1.84	n.d.
Total	100.00	99.21

* X-ray fluorescence analysis using the method of Hooper and Atkins (1969) normalized to 100 wt%.
** Owing to the highly oxidizing conditions under which this rock formed, all Fe reported as Fe^{3+}.
† Number of point analyses equal to 20.

and specific-gravity methods, into fractions for detailed powder-diffraction analysis. Precision lattice parameters for two of the mineral separates (pyroxene and melilite) were obtained by least-squares refinement of Cu*Kα diffractometer data, which were internally calibrated with NaCl.*

The whole-rock chemistry of the buchite was determined by mixing a representative 3.5-g sample ground to 200 mesh with 7 g of lithium tetraborate and fusing it into a bead (Hooper and Atkins, 1969), which was subsequently analyzed using a Philips P.W. 1410 X-ray spectrograph.

Mineralogy, chemistry, and petrography

Petrographic examination and X-ray powder-diffraction analysis of the reddish-brown siliceous shale in contact with the buchite revealed the presence of mullite, cristobalite, tridymite, hematite, and relic detrital quartz, a mineral assemblage similar to that observed in the thermally altered shales at Kemmerer, Wyoming (Hooper, 1982).

The various hues present in the vesiculated buchite are the product of fine-scale variations in the minerals present; the green portions are rich in pyroxene, the black portions are rich in iron oxides, and the orange-red portions are rich in melilite and silicate glass. The gas vesicles are lined with druzy orange silicate glass or with a fine matte of feldspar, pyroxene, or iron oxide crystals. Macroscopic examination of broken surfaces reveals a color and mineral zoning concentric about the gas vesicles in many places.

The bulk sample and associated glass (Table 1) are significantly lower in silica and higher in alumina and ferric iron than buchites described from the Kemmerer coal burn (Hooper, 1982; Hooper et al., 1986), which may, in part, explain its unusual mineral assemblage.

In thin section, the buchite consists of an intimate mixture (in decreasing order of abundance) of anorthite, clinopyroxene, iron oxides (magnesioferrite and hematite), melilite, and silicate glass. Most of the crystalline phases are euhedral with crystal sizes varying from several micrometers to several millimeters. In some places, stringers of melilite and magnesioferrite crystals contained in a pyroxene groundmass loop around large pyroxene crystals as well as around gas vesicles, suggestive of viscous flow of a crystalline mush. In other areas, micrometer-sized melilite riddles both the large pyroxene crystals as well as the fine-grained anorthite and glass groundmass. Mineral zoning around gas vesicles is also evident in thin section. One particularly well-developed example consists of a black oxide vesicle lining, surrounded by a layer of reddish-brown melilite, which in turn is encased in a mass of yellow-green pyroxene.

The iron oxides range in size from tiny euhedral crystals to large irregular masses and stringers hundreds of micrometers long. Virtually all of the oxide masses and euhedra, regardless of size, have components with high (hematite) and low (magnesioferrite) reflectivity. The smaller masses and euhedra frequently have a high-reflectivity core and a lower-reflectivity rim, whereas the larger masses may consist of highly reflective lamellae or numerous geometrically arranged blebs encased in a lower-reflectivity host reminiscent of the Fe-Ti oxide intergrowths described by Haggarty (1976).

The clinopyroxene is moderately pleochroic in hues of pale green (α) and bright straw yellow (β and γ). It displays a relatively high birefringence (0.025–0.030) and unlike most Fe-rich clinopyroxenes is optically negative with $2V_X = 65$–$75°$. The most striking optical property of the small (~0.5 mm) tabular melilite crystals is their intense color and very high birefringence (>0.040). The Fe-rich melilites are moderately pleochroic from dark reddish-brown to orange-brown, whereas the more aluminous melilites have a yellowish-brown (ϵ) to olive green (ω) pleochroism. No gradation in color corresponding to compositional intermediates was observed. The melilites appear to be optically negative over the entire range of observed composition. The optical properties of the isotropic magnesioferrite crystals are equally variable. The Fe-rich magnesioferrites are generally opaque in thin section, although very thin crystals display a deep blood-red

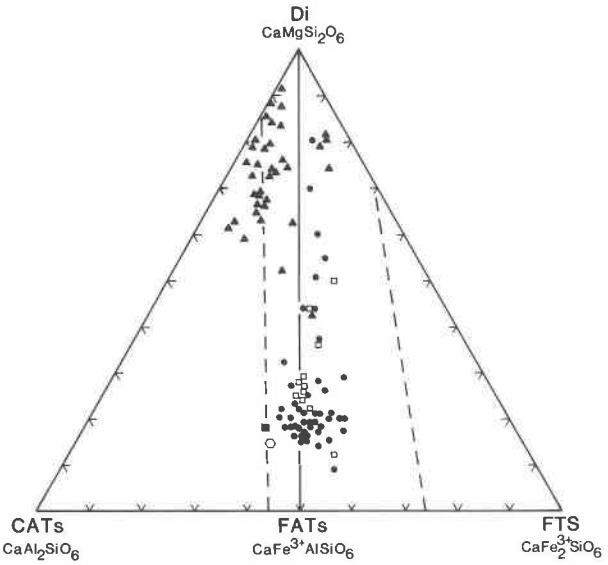

Fig. 2. The compositions of clinopyroxenes from the I-90 buchite (● = 1 point analysis per crystal and □ = multiple point analyses per crystal) and fassaites and fassaitic augites (▲) taken from the literature by Huckenholz et al. (1974). The hexagon and filled square represent buchite clinopyroxene compositions reported by Cosca and Essene (1985) and Cosca et al. (1985). The diagram is a modification of Fig. 19 in Huckenholz et al. (1974). Dashed lines define the area of clinopyroxene solid solutions at low pressure (see Huckenholz et al., 1974, for details).

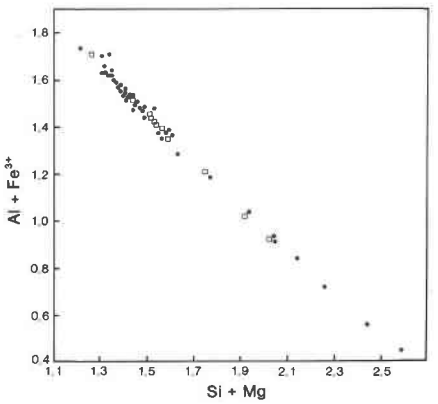

Fig. 3. The variation of Al + Fe^{3+} with Si + Mg for the I-90 pyroxene (● = 1 point analysis per crystal and □ = multiple point analyses per crystal). Numbers of ions based on six oxygens.

color. The more aluminous magnesioferrites are transparent and range in color from orange to colorless. The unusual optical properties of the clinopyroxene and melilite, suggestive of an interesting chemistry, provided the impetus for this investigation.

Clinopyroxene

Mineral chemistry

The variations in clinopyroxene optical properties observed in thin section are correlated to variations in Fe and Al content that are observed over hundreds or in places tens of micrometers. In general, the deeper shades of green and the more marked pleochroism are associated with higher Fe contents. The clinopyroxene microprobe data are presented assuming Fe in the trivalent state. This is consistent with the extremely oxidizing conditions of formation and calculated structural formulas with extremely small to nonexistent cation deficiencies (Cawthorn and Collerson, 1974). Ca is nearly stoichiometric, 0.92–1.00 cations per formula unit (pfu), and Ti and Na are present in only minor amounts, 0.02–0.04 cations pfu.

Microchemical analysis of approximately 70 crystals revealed a wide range of chemical variability from Fe^{3+}- and Al-poor, Si- and Mg-rich compositions (crystal 94, Table 2; Fig. 2) approaching endmember diopside (Di, $CaMgSi_2O_6$) to Fe^{3+}- and Al-rich, Si- and Mg-poor compositions (crystal 65, Table 2; Fig. 2) approaching ferri-aluminum Tschermaks component (FATs; $CaFeAlSiO_6$). The observed compositional variability (Fig. 2) is restricted to the area of clinopyroxene solid solution at low pressure that straddles the Di-FATs join in the Di–CaTs ($CaAl_2SiO_6$)–FTs ($CaFe^{3+}_2SiO_6$) system (Huckenholz et al., 1974). Thus, the compositional variability of these clinopyroxenes largely conforms to the coupled substitution $Si^{4+} + Mg^{2+} = Fe^{3+} + Al^{3+}$ (Fig. 3). Only crystals with compositions approaching FATs exhibited measurable chemical zoning as is reflected in the standard deviations of oxide weight percentages obtained for crystal 52 (Table 2).

Many of the clinopyroxene crystals have higher Fe^{3+} and Al contents and lower Si contents than any natural pyroxene (e.g., fassaites) previously reported (Majmundar, 1971; Mason, 1974; Devine and Sigurdsson, 1980; Fig. 2) including two from another coal-fire buchite in the Powder River Basin of Wyoming (Cosca and Essene, 1985; Cosca et al., 1985). Although Cosca et al. (1985) reported compositions ranging from diopside to "near end member ferri-aluminum Tschermaks," the chemical compositions (see also Cosca and Essene, 1985) are displaced from this join toward CATS (Fig. 2). A complete range of substitution between Di and FATs in coal-fire buchites is to be expected since the experimental studies of Hijikata and Onuma (1969) and Huckenholz et al. (1974) reveal complete solid solution between Di and FATs and between $FTs_{78}CaTs_{22}$ and $FTs_{48}CaTs_{52}$, respectively, above 1100°C at 1 atm.

If cation occupancies are assigned assuming that Si deficiencies in the tetrahedral site are compensated by Al and that any remaining deficiency is compensated by Fe^{3+} (Hartman, 1969; Ohashi and Hariya, 1973; Ghose et al., 1975; Huggins et al., 1977), then for most of the crystals, virtually all of the available Al and generally a small amount of Fe^{3+} (<0.17 cations pfu) are in tetrahedral coordination. The preference of the tetrahedral site for Al over Fe^{3+} is reflected in the trends in the chemical data. Crystals with higher Fe^{3+}/Al atom ratios (>1.5) have more Si (less Al) in the tetrahedral site (Fig. 4). Conversely, in

Table 2. Electron-microprobe analyses of Fe^{3+}-rich clinopyroxene in the buchite

	Crystal* 52	Crystal 65	Crystal 94	Composite of 74 crystals
		Weight percent		
SiO_2	27.72(1.15)	26.70	47.12	32.28(4.35)
Al_2O_3	15.14(1.08)	15.21	3.96	14.13(3.24)
TiO_2	1.04(23)	0.74	0.54	0.91(22)
Fe_2O_3**	31.86(2.47)	32.35	9.98	25.21(4.60)
MgO	1.92(47)	1.44	14.22	4.45(2.61)
MnO	0.08(4)	0.05	0.25	0.13(8)
CaO	22.64(24)	22.73	22.98	23.06(29)
Na_2O	0.24(14)	0.16	0.44	0.32(15)
K_2O	0.00	0.00	0.01	0.02(3)
Total	100.67(54)	99.38	99.50	100.51(63)
		Cations per six oxygen		
Si	1.13	1.11	1.77	1.29
Al	0.73	0.74	0.18	0.65
Ti	0.03	0.02	0.02	0.02
Fe^{3+}	0.98	1.01	0.28	0.76
Mg	0.12	0.09	0.80	0.26
Mn	—	—	0.01	—
Ca	0.99	1.01	0.93	0.98
Na	0.02	0.01	0.03	0.02
K	—	—	—	—

Formulas assuming a tetrahedral-site preference Si > Al > Fe^{3+}

Crystal 52: $(Ca_{0.99}Na_{0.01})(Fe^{3+}_{0.84}Mg_{0.12}Ti_{0.03}Na_{0.01})(Si_{1.13}Al_{0.73}Fe^{3+}_{0.14})O_6$

Crystal 65: $(Ca_{1.00})(Fe^{3+}_{0.86}Mg_{0.09}Ti_{0.02}Na_{0.01}Ca_{0.01}\square_{0.01})(Si_{1.11}Al_{0.74}Fe^{3+}_{0.15})O_6$

Crystal 94: $(Ca_{0.93}Na_{0.03}Mg_{0.05})(Mg_{0.75}Fe^{3+}_{0.23}Ti_{0.02})(Si_{1.77}Al_{0.18}Fe^{3+}_{0.05})O_6$

Composite: $(Ca_{0.98}Na_{0.02})(Fe^{3+}_{0.70}Mg_{0.26}Ti_{0.02}\square_{0.02})(Si_{1.29}Al_{0.65}Fe^{3+}_{0.06})O_6$

* Average of 13 point analyses on the same crystal.

** Fe assumed to be in the trivalent state because (1) of the extremely oxidizing conditions of clinopyroxene formation and (2) cation totals are or are very nearly stoichiometric for all of the crystals analyzed.

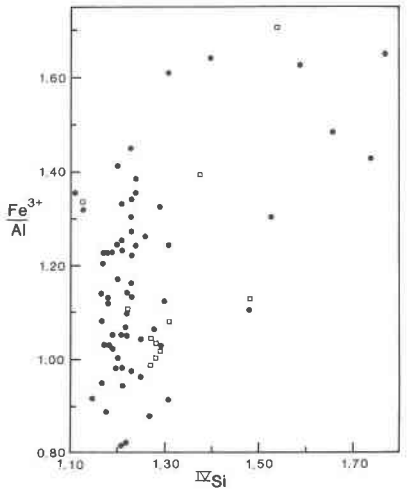

Fig. 4. The variation of Si with the Fe^{3+}/Al atom ratio (● = 1 point analysis per crystal and □ = multiple point analyses per crystal). Numbers of ions based on six oxygens.

crystals having lower Fe^{3+}/Al atom ratios (<1.5), the tetrahedral site is usually more deficient in Si, allowing the inclusion of more Al. This is not to imply that at high Fe^{3+}/Al atom ratios there is no $^{IV}Fe^{3+}$. In almost all of the crystals there is insufficient Si and Al to fill the tetrahedral sites. A high positive correlation, $r = 0.83$, between the tetrahedral site deficiency and the Fe^{3+}/Al atom ratio (Fig. 5) suggests that in crystals having the highest ratio, a small amount of Fe^{3+} (<0.17 atoms pfu) is in tetrahedral coordination. The crystals lying above the dashed line in Figure 5 have the highest Si and Mg contents (Si + Mg > 2.0 atoms pfu). The high Si content of these crystals results in a smaller than expected tetrahedral deficiency ($^{IV}\square$) and, therefore, a smaller than expected amount of Fe^{3+} substitution in the tetrahedral sites despite their very high Fe^{3+}/Al ratios.

Although X-ray structural studies of natural Fe^{3+}- and Al-rich clinopyroxenes (Peacor, 1967; Hazen and Finger, 1977; Cosca et al., 1985) have not revealed the presence of $^{IV}Fe^{3+}$, crystal-chemical considerations (Hartman, 1969) and X-ray structure and ^{57}Fe Mössbauer studies indicate that some Fe^{3+} substitution in clinopyroxene tetrahedral sites is possible. A Mössbauer spectral analysis of silica-deficient clinopyroxenes on the join $CaFe^{3+}AlSiO_6$-$CaTiAl_2O_6$ (Akasaka, 1983) and an X-ray structure analysis of synthetic clinopyroxene of FATs composition, $CaFe^{3+}AlSiO_6$, (Ghose et al., 1975), revealed that 4.5–9.0% of the tetrahedral sites are occupied by Fe^{3+}, a range comparable to the 0–8.5% observed for the buchite clinopyroxenes from Buffalo, Wyoming. Likewise, Kurepin et al. (1981) reported that only ⅔ of the octahedral sites in a FATs pyroxene ($CaFe^{3+}AlSiO_6$) synthesized at 1200°C are occupied by Fe^{3+}, implying that 17% of the tetrahedral sites are occupied by Fe^{3+}. A silica-deficient, Al- and Fe^{3+}-rich clinopyroxene identified in iron ore sinters (Dyson and Juckes, 1972) requires the presence of Fe^{3+} in up to 16% of the tetrahedral sites.

It is not surprising in light of our data that the ferri-aluminum clinopyroxene, $(Ca_{1.01}Na_{0.01})(Fe_{0.65}Mg_{0.18}Al_{0.10}Ti_{0.03}Fe_{0.02})(Al_{0.79}Si_{1.21})O_6$, from a Wyoming coal-fire buchite examined by Cosca et al. (1985) did not contain detectable $^{IV}Fe^{3+}$ The Fe^{3+}/Al atom ratio in this clinopyroxene is 0.73, which is in the range of ratios for crystals in which apparently no $^{IV}Fe^{3+}$ is present (Fig. 5), and this crystal contains sufficient Si and Al to completely fill the tetrahedral site. The amount of $^{IV}Fe^{3+}$ is very low (<9% of the tetrahedral sites) even in the clinopyroxenes that have relatively high Fe^{3+}/Al atom ratios (1.0–1.7).

X-ray data

Enough ferri-aluminum clinopyroxene for an X-ray powder-diffraction analysis internally calibrated with NaCl was obtained through heavy-liquid and magnetic separation techniques. The indexed pattern is presented in Table 3. Least-squares refinement of the unit-cell parameters in space group $C2/c$ (Cosca et al., 1985) using the 18 most intense reflections yielded $a = 9.793(3)$ Å, $b = 8.835(4)$ Å, $c = 5.326(4)$ Å, $\beta = 105.84(4)°$ and cell volume = 443.3(3) Å^3. These parameters and cell volume (Table 3) are close to those obtained for a synthetic Fe^{3+}- and Al-rich clinopyroxene, $Ca(Fe_{0.5}Mg_{0.4}Ti_{0.1})(Al_{0.7}Si_{1.3})O_6$ (Akasaka and Onuma, 1980), having a similar composition but are significantly larger than those of synthetic FATs, $CaFe^{3+}AlSiO_6$, (Huckenholz et al., 1974). The

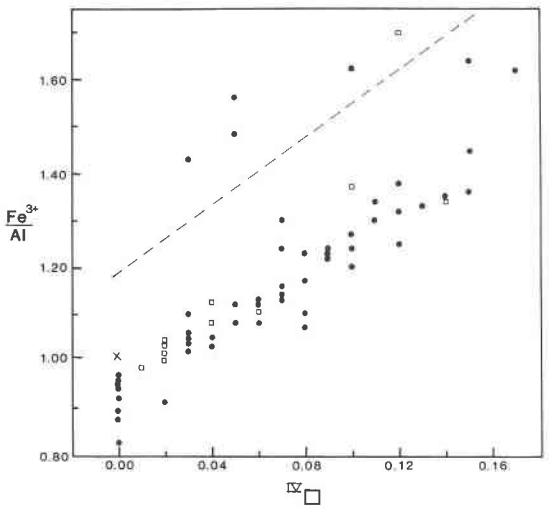

Fig. 5. The variation of inferred tetrahedral site deficiency ($^{IV}\square$) with the Fe^{3+}/Al atom ratio (● = 1 point analysis per crystal and □ = multiple point analyses per crystal). $^{IV}\square = 2.0 - (Si + Al)$ with numbers of ions based on six oxygens per formula unit. Crystals lying above the dashed line have a high Si + Mg content (Si > 1.50 atoms pfu, Mg > 0.49 atoms pfu) whereas those below have a low Si + Mg content (Si < 1.50 atoms pfu and Mg < 0.45 atoms pfu). $X = Fe^{3+}/Al$ ratio in FATs.

smaller c unit-cell parameter of the ferri-aluminum clinopyroxene compared to FATs clinopyroxene is due to the replacement of Al^{3+} by the smaller Si^{4+} in the tetrahedral chain, whereas the larger b and c parameters are due to the replacement of Fe^{3+} and Al^{3+} in the M1 site by the larger Mg^{2+} cation. The angle β is largely unchanged because of the complete occupancy of the M2 site by Ca in all three of these clinopyroxenes (Huckenholz et al., 1974).

Melilite

Mineral chemistry

Most melilites are solid solutions of åkermanite—$Ca_2(MgSi_2O_7)$, gehlenite—$Ca_2(Al_2SiO_7)$, Fe åkermanite—$Ca_2(Fe^{2+}Si_2O_7)$, and Na melilite—$NaCa(AlSi_2O_7)$ and occur in undersaturated igneous rocks, thermally metamorphosed impure carbonates, and blast furnace slags (Deer et al., 1963). Although melilites close in composition to these ideal endmembers are rare in nature, all of the endmembers (åkermanite, Osborn and Schairer, 1941; gehlenite, Yoder, 1950; Fe åkermanite, Bowen et al., 1933; Na melilite, Nurse and Midgley, 1953) have apparently been synthesized. Seifert (1974) has suggested that Fe åkermanite is not stable and that a maximum solid solution of 80% Fe åkermanite in åkermanite is achieved at 1170°C and 1 atm. Moreover, Huckenholz and Ott (1978) have reported that $Fe^{3+} \rightarrow Al^{3+}$ substitution in gehlenite reaches a maximum of 37.5 wt% of the ferrigehlenite component ($Ca_2Fe^{3+}_2SiO_7$) at 1237°C and 1 atm and that Fe gehlenite ($Ca_2Fe^{3+}AlSiO_7$) is not stable at any temperature in the pressure range 1 atm to 7 kbar.

Table 3. X-ray powder-diffraction pattern and least-squares refined cell parameters of the Fe^{3+}-rich pyroxene and the synthetic Fe^{3+}-rich pyroxene of Akasaka and Onuma (1980)

	Fe^{3+}- and Al-rich clinopyroxene			Fassaite**	
hkl	d_{obs} (Å)	I/I_0	d_{calc} (Å)	d_{calc} (Å)	I/I_0
110	6.43	15	6.4444	6.471	4
200	4.71	10	4.7104	4.710	6
020	4.43	10	4.4174	4.453	5
111	3.77	5	3.6888	3.689	1
220	3.2155*	55	3.2222	3.236	17
$\bar{2}21$	3.0007*	95	2.9909	3.002	100
310	2.9589*	100	2.9589	2.961	33
$\bar{3}11$	2.9022*	20	2.9065	2.909	27
$\bar{1}31$	2.5731*	20	2.5536	2.568	31
$\bar{2}02$	2.5603*	40	2.5632	2.561	46
002			2.5616	2.558	
221	2.5238*	75	2.5234	2.528	42
311	2.3174*	15	2.3171	2.316	12
112	—	—	—	2.239	11
$\bar{2}22$	—	—	—	2.220	
022	—	—	—	2.218	8
330	2.1460*	37	2.1481	2.157	9
$\bar{3}31$	2.1290*	41	2.1278	2.137	19
$\bar{4}21$	2.1128*	17	2.1111	2.115	11
041	—	—	—	2.042	14
$\bar{4}02$	2.0321*	17	2.0321	2.032	14
202	1.9956	17	2.0298	2.027	15
$\bar{1}32$			1.9751	1.9809	6
510	1.8421*	22	1.8427	1.8431	5
150	1.7372*	20	1.7367	1.7502	11
$\bar{1}51$	—	—	—	1.6824	7
$\bar{3}13$	1.67	5	1.6777	1.6794	6
042			1.6728	1.6769	7
$\bar{2}23$	1.64	10	1.6411	1.6413	14
$\bar{5}31$	1.6248*	32	1.6254	1.6295	12
440	1.6111*	24	1.6111	1.6178	5
600	1.56	5	1.5701	1.5699	3
$\bar{6}02$	1.5394*	17	1.5389	1.5391	6

	Fe^{3+}- and Al-rich clinopyroxene	Synthetic Fe^{3+}- and Al-rich clinopyroxene†	Synthetic FATs‡
a (Å)	9.793(3)	9.771(2)	9.751(9)
b (Å)	8.835(4)	8.843(2)	8.781(8)
c (Å)	5.326(3)	5.334(1)	5.360(8)
β (°)	105.84(3)	106.01(2)	105.87(8)
V (Å^3)	443.3(3)	443.0(2)	441.4(7)

* Reflections used in least-squares refinement of unit-cell parameters.

** Fassaite data from Borg and Smith (1969; p. 250–252). Reflections with $I/I_0 < 5$ that do not correspond to observed Fe^{3+}-rich clinopyroxene reflections have been omitted.

† Having composition $Ca(Fe_{0.5}Mg_{0.4}Ti_{0.1})(Si_{1.3}Al_{0.7})O_6$ (Akasaka and Onuma, 1980).

‡ Huckenholz et al., 1974.

The buchite melilite is unusual in that many of the crystals are richer in Fe^{3+} (Fe_2O_3 averages 46.14 wt% with a maximum of 60.09 wt%, Table 4) and poorer in Si and Ca than the endmember ferrigehlenite (Fe_2O_3 = 48.11 wt%); this is a result of the coupled substitution $Fe^{3+} + Al^{3+} = Si^{4+} + R^{2+}$, which displaces compositions from the "gehlenite-ferrigehlenite" join, $R^{2+}_2(Al_2SiO_7)R^{2+}_2$-$(Fe^{3+}_3SiO_7)$, toward the hypothetical endmember $R^{2+}R^{3+}(R^{3+}_3O_7)$ (Fig. 6). The major compositional variability in these melilites involves $Fe^{3+} \rightarrow Al^{3+}$ substitution with very little variability in Si, Mg, or Ca, which is reflected in the small standard deviations of the analyses

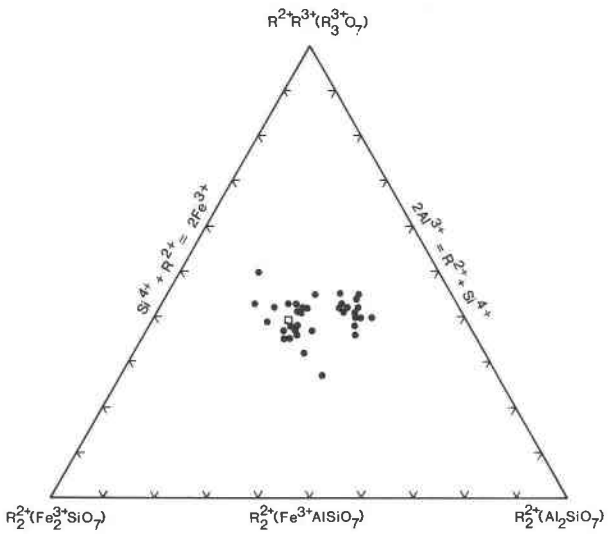

Fig. 6. The compositions of melilite from the I-90 buchite. Melilite compositions plotted on the basis of assumed tetrahedral-site occupancies (● = 1 point analysis per crystal and □ = multiple point analyses per crystal). $R^{2+}_2(Al_2SiO_7)$ = "gehlenite," $Ca_2Fe^{3+}AlSiO_7$ = "Fe gehlenite," $R^{2+}_2(Fe^{3+}_2SiO_7)$ = "ferri-gehlenite" where R^{2+} = principally Ca.

(Table 4) and the limited range in Si + Mg and Fe^{3+} + Al cation totals (Fig. 7). This is in sharp contrast to the wide variation in Si, Mg, Al, and Fe^{3+} in the clinopyroxenes due to $Fe^{3+} + Al^{3+} \rightarrow Si^{4+} + Mg^{2+}$ coupling along the Di-FATs join. The absence of melilite compositions that approach endmember ferrigehlenite or Fe gehlenite supports the contention of Huckenholz and Ott (1978) that these phases are not stable at 1 atm. There is very little compositional zoning in these melilite crystals, as demonstrated by the small standard deviations of oxide weight percentages of random point analyses of a single crystal (Table 4).

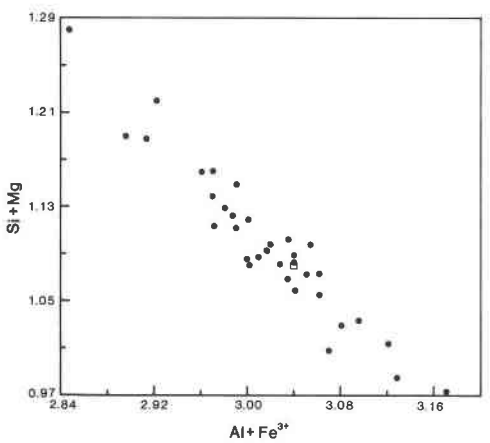

Fig. 7. The variation of Fe^{3+} + Al with Si + Mg in melilites from the I-90 buchite (● = 1 point analysis per crystal and □ = multiple point analyses per crystal).

Table 4. Electron-microprobe analyses of Fe^{3+}-rich melilites

	Composite			
	1	2		
	Single crystal*	36 crystals**	36 crystals	High Al melilite	High Fe^{3+} melilite
	Weight percent				
SiO_2	11.85(21)	11.73(1.27)	11.73	12.55	9.36
Al_2O_3	17.30(50)	21.09(5.03)	21.09	29.56	11.85
TiO_2	0.42(3)	0.91(48)	0.91	1.60	0.57
Fe_2O_3	51.31(90)	46.14(6.22)	42.01	36.97	60.09
Cr_2O_3	n.d.	0.05(3)	0.05	0.02	0.00
FeO	—	—	3.72	—	—
MnO	0.21(6)	0.23(10)	0.23	0.14	0.35
NiO	n.d.	0.02(2)	0.02	0.02	0.02
MgO	6.14(25)	6.96(1.16)	6.96	6.74	5.91
CaO	12.74(9)	12.95(34)	12.95	13.47	12.33
Na_2O	0.31(6)	0.31(11)	0.31	n.d.	n.d.
K_2O	0.03(3)	0.02(2)	0.02	n.d.	n.d.
Total	100.31(50)	100.41(71)	100.00	101.07	100.50
	Cations per seven oxygens				
Si	0.61	0.59	0.60	0.60	0.50
Al	1.05	1.25	1.26	1.67	0.75
Ti	0.02	0.03	0.03	0.06	0.02
Fe^{3+}	1.99	1.75	1.61	1.33	2.42
Cr^{3+}	—	tr.	tr.	tr.	tr.
Fe^{2+}	—	—	0.16	—	—
Mn	0.01	0.01	0.01	0.01	0.02
Ni	—	tr.	tr.	tr.	tr.
Mg	0.47	0.53	0.53	0.48	0.47
Ca	0.70	0.70	0.71	0.69	0.71
Na	0.03	0.03	0.03	—	—
K	tr.	tr.	tr.	—	—

Formulas

Single crystal: $(Ca_{0.70}Fe^{3+}_{0.65}Mg_{0.47}\square_{0.12}Na_{0.03}Ti_{0.02}Mn_{0.01})(Fe^{3+}_{1.34}Al_{1.04}Si_{0.61})O_7$
Composite 1: $(Ca_{0.70}Fe^{3+}_{0.59}Mg_{0.53}\square_{0.11}Na_{0.03}Ti_{0.03}Mn_{0.01})(Fe^{3+}_{1.16}Al_{1.25}Si_{0.59})O_7$
Composite 2:
$(Ca_{0.71}Fe^{3+}_{0.47}Fe_{0.16}Mg_{0.53}\square_{0.06}Na_{0.03}Ti_{0.03}Mn_{0.01})(Fe^{3+}_{1.14}Al_{1.26}Si_{0.60})O_7$
High-Al melilite: $(Ca_{0.69}Fe^{3+}_{0.60}Mg_{0.48}\square_{0.16}Ti_{0.06}Mn_{0.01})(Fe^{3+}_{0.73}Al_{1.67}Si_{0.60})O_7$
High-Fe melilite: $(Ca_{0.71}Fe^{3+}_{0.67}Mg_{0.47}\square_{0.11}Ti_{0.02}Mn_{0.02})(Fe^{3+}_{1.75}Al_{0.75}Si_{0.50})O_7$

Note: Values in parentheses are the standard deviations. Total Fe reported as Fe^{3+}.

* Values represent the mean of 8 point analyses on this crystal.

** Values represent the mean of 36 point analyses on 36 different crystals.

Assignment of the available (Si,Al) and Ca atoms to the tetrahedral and eight-coordinated sites, respectively, in compliance with the structural data of Louisnathan (1971) and Kimata and Ii (1982), leaves these sites slightly cation deficient. Although Mg is normally found in tetrahedral coordination in melilites (åkermanite; Kimata and Ii, 1981), it was assigned to the eight-coordinated site because it is appreciably larger than Fe^{3+}, leaving the remaining tetrahedral sites to be filled by Fe^{3+} (Table 4). This is consistent with the site assignments for compositions synthesized on the gehlenite-ferrigehlenite join (Huckenholz and Ott, 1978). Even if all the available Si, Al, and Mg were placed in tetrahedral coordination, a significant Fe^{3+} occupancy of the tetrahedral sites would still be required. Assigning the cations according to this scheme leads to nearly a constant ratio of Ca : Mg : Fe^{3+} in the eight-coordinated site and a variable Fe^{3+} : Al ratio in the tetrahedral sites.

A significant cation deficiency is common to all of the melilite structural formulas. Partitioning of the total Fe

Table 5. X-ray powder-diffraction patterns and least-squares refined unit-cell parameters of Fe^{3+}-rich melilite and gehlenite

	Fe^{3+}-rich melilite This study			Gehlenite Louisnathan (1971)		
hkl	d_{obs} (Å)	I/I_0	d_{calc} (Å)	d_{obs} (Å)	I/I_0	d_{calc} (Å)
110	—	—	5.4556	5.449	5	5.457
001	—	—	5.0993	5.081	5	5.087
101	—	—	4.2541	4.231	9	4.247
111	3.7160	18	3.7254	3.711	28	3.721
210	—	—	3.4504	3.475	2	3.451
201	3.0791	24	3.0765	3.066	27	3.074
211	2.8577	100	2.8577	2.848	100	2.856
220	—	—	2.7278	2.738	15	2.729
002	—	—	2.5497	2.547	15	2.543
310	2.4530	24	2.4398	2.437	32	2.441
102	—	—	2.4209	2.421	12	2.415
221	2.4069	21	2.4053	2.408	30	2.405
112	2.3116	24	2.3099	2.314	4	2.305
301	—	—	2.2963	2.291	19	2.296
311	—	—	2.2009	2.206	3	2.200
202	—	—	2.1271	2.117	4	2.125
212*	—	—	2.0506	2.038	10	2.047
321	1.9785	14	1.9704	1.970	4	1.973
400**	—	—	1.9288	1.921	55	1.929
410	—	—	1.8713	1.876	8	1.872
222	—	—	1.8627	1.865	4	1.860
330**	—	—	1.8185	1.818	55	1.819
302	—	—	1.8107	1.812	7	1.809
312	1.7619	27	1.7628	1.768	45	1.761

	Gehlenite Louisnathan (1971)	Fe^{3+}-rich gehlenite Huckenholz and Ott (1978)	Fe^{3+}-rich melilite This study†
a (Å)	7.706(5)	7.712	7.715(9)
c (Å)	5.069(7)	5.081	5.099(6)
V (Å³)	301.0	302.2	303.6(5)
c/*a*	0.658	0.659	0.661

* This reflection was listed as 122 by Louisnathan (1971).

** These reflections were masked by those of the Fe^{3+}-rich pyroxene that was also present in the sample.

† All observed reflections were used in the least-squares refinement.

into the two valence states in such a way as to reduce the composite (36 crystals) analytical total to 100 wt% results in a $Fe^{3+}:Fe^{2+}$ ratio of 10 and a significantly reduced cation deficiency in the calculated formulas (Table 4). This suggests that a small and probably variable amount of Fe^{2+} is present in these melilites.

X-ray data

The X-ray powder-diffraction pattern of the buchite melilite is very similar to that of gehlenite (Table 5). The least-squares refined unit-cell dimensions and volume are somewhat larger than those of endmember gehlenite (Louisnathan, 1971) and the most Fe^{3+}-rich gehlenite (37.5 mol% ferrigehlenite, $Fe_2O_3 \approx 18$ wt%) synthesized by Huckenholz and Ott (1978) at 1400°C and 1 atm. Huckenholz and Ott (1978) observed an increase of approximately 2% in cell volume and nearly constant *c*/*a* lattice parameter ratios (0.658 ± 0.001) over the compositional range from 0 to 37.5 mol% ferrigehlenite for samples synthesized at 1 atm on the gehlenite-ferrigehlenite join. The larger *c*/*a* ratio (0.661, Table 5) in the buchite melilite may reflect Fe^{3+} substitution in both the eight- and four-coordinated sites, which is required by compositional variation extending from the gehlenite-ferrigehlenite join toward $R^{2+}R^{3+}(R^{3+}_3O_7)$, rather than in just the four-coordinated sites as required by compositional variation along the join. A better understanding of how the melilite structure accommodates the extensive substitution of Fe^{3+} in sites of different coordination is the focus of X-ray structural studies currently underway.

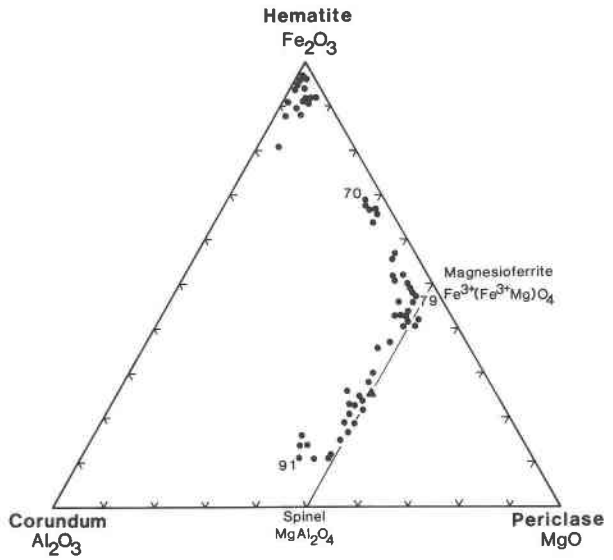

Fig. 8. The compositions of the oxides in the buchite [● = 1 point analysis per crystal and ▲ = $(Al_{0.5}Fe^{3+}_{0.5})(MgAl_{0.5}Fe^{3+}_{0.5})O_4$; Bacon and Welch, 1954]. Numbered points correspond to analyses in Table 7.

Iron oxides

Mineral chemistry

Three types of oxides were observed in this sample; abundant Al- and Mg-rich hematites and aluminous magnesioferrites and minor pseudobrookite.

The hematite occurs both as discrete crystals and as intergrowths with the magnesioferrite. The hematite chemistry is variable (Fig. 8); every crystal analyzed contains Al and Mg and many also contain minor amounts of Na, Ca, Si, Mn, Ni, Cr, and Ti (Table 6). A maximum substitution of 15 mol% Al_2O_3 and 6 mol% MgO was observed in crystal 82 (Table 6). Although aluminous hematites have been reported in soils (Schwertmann et al., 1977; Bigham et al., 1978) and bauxite deposits (Solymar and Jonas, 1971), these coal-burn hematites represent the most Al-rich natural hematites reported to date.

Numerous experimental investigations of Al substitution in hematite have been conducted over a wide range of temperatures using diverse starting materials and preparation techniques. The 15 mol% maximum substitution observed in crystal 82 compares favorably with the 15–18 mol% solubility limit observed by Muan and Gee

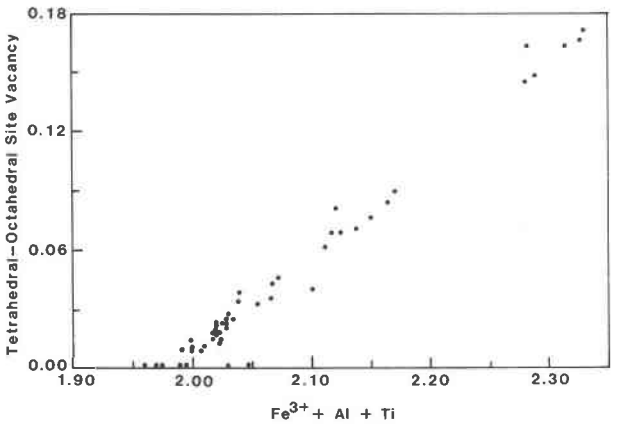

Fig. 9. Variation of the tetrahedral- and octahedral-site vacancies with Fe^{3+} + Al + Ti^{4+} substitution in the magnesioferrites (● = 1 point analysis per crystal).

(1956), von Steinwehr (1967), Schwertmann et al. (1979), Fysh and Clark (1982), and Barron et al. (1984) for aluminous hematites prepared by firing ferrihydrates and oxide-hydroxide mixtures in the temperature range 400–1000°C. Al_2O_3 (3–5 mol%) appears to "strengthen" the hematite structure by "strain relief through small amounts of smaller Al cations in the octahedral lattice sites" (DeGrave et al., 1985; Schwertmann et al., 1979).

In contrast to the hematites, the magnesioferrites exhibit a considerable range of compositional variability

Table 6. Electron-microprobe analyses of hematites

	Crystal 82	Crystal 80	Composite of 21 crystals
	Weight percent		
SiO_2	0.78	0.06	0.10(15)
Al_2O_3	9.70	1.22	2.87(1.78)
TiO_2	2.31	0.15	2.08(1.40)
Fe_2O_3	83.02	96.60	92.81(2.95)
Cr_2O_3	0.00	0.00	0.04(5)
MnO	0.20	0.40	0.20(9)
NiO	0.00	0.00	0.02(3)
MgO	1.15	0.25	0.93(57)
CaO	0.15	0.04	0.19(31)
Na_2O	0.00	0.09	0.03(4)
K_2O	0.05	0.00	0.01(1)
Total	97.36	98.80	99.28(75)
	Cations per three oxygens		
Si	0.02	tr.	tr.
Al	0.29	0.04	0.09
Ti	0.04	tr.	0.04
Fe^{3+}	1.59	1.94	1.82
Cr	—	—	tr.
Mn	tr.	0.01	0.02
Ni	—	—	tr.
Mg	0.04	0.01	0.04
Ca	tr.	tr.	0.01
Na	—	tr.	tr.
K	tr.	—	tr.

Formulas

Crystal 82: $(Fe^{3+}_{1.59}Al_{0.29}Mg_{0.04}Ti_{0.04}Si_{0.02}\square_{0.02})O_3$

Crystal 80: $(Fe^{3+}_{1.94}Al_{0.04}Mg_{0.01}Mn_{0.01})O_3$

Composite: $(Fe^{3+}_{1.82}Al_{0.09}Mg_{0.04}Ti_{0.04}Mn_{0.02}Ca_{0.01})O_3$

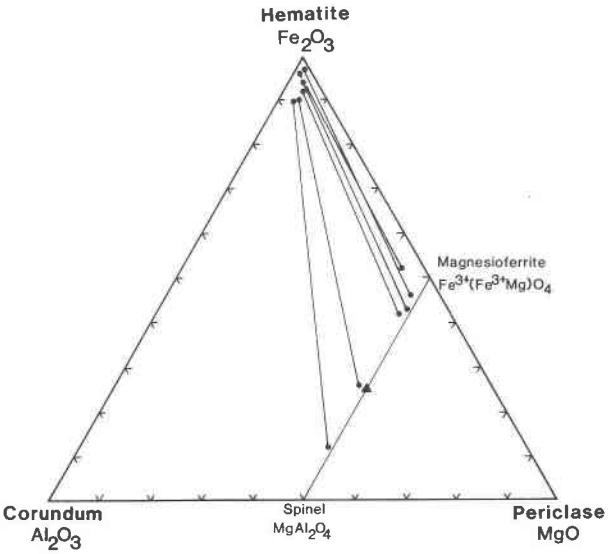

Fig. 10. Compositions of coexisting hematite and magnesioferrite solid solutions [● = 1 point analysis per crystal and ▲ = $(Al_{0.5}Fe_{0.5})(MgAl_{0.5}Fe_{0.5})O_4$; Bacon and Welch, 1954].

(Fig. 8), extending from $(Al_{0.72}Fe^{3+}_{0.21}\square_{0.07})(Al_{0.97}Mg_{0.79}\cdot Fe^{3+}_{0.22}\ Mn_{0.01}Cr_{0.01})O_4$ (composition 91, Table 7) beyond the synthetic phase $(Al_{0.5}Fe^{3+}_{0.5})(MgAl_{0.5}Fe^{3+}_{0.5})O_4$ (Bacon and Welch, 1954) to $(Fe^{3+}_{0.91}Al_{0.08}\square_{0.01})(Mg_{0.94}Fe^{3+}_{0.92}\cdot Al_{0.10}Mn_{0.04})O_4$ (composition 79, Table 7), thence to composition $Fe^{3+}_{2.21}Mg_{0.43}Al_{0.11}Mn_{0.05}Ti_{0.01}Ca_{0.01}\square_{0.18})O_4$ (composition 70, Table 7) approximately midway along the hematite-magnesioferrite join. The total concentration of other elements, notably Ti, Ni, and Cr in these samples rarely exceeds 2 wt%.

Most crystals are Al rich, slightly defective, and do not lie on their respective joins (Fig. 8) owing to substitution of the type $2(Al^{3+},Fe^{3+}) + \square = 3Mg^{2+}$. This is clearly demonstrated by the high linear correlation (r = 0.99) between total (Al + Fe^{3+} + Ti^{4+}) and the total tetrahedral and octahedral site vacancy (Fig. 9). Crystals having compositions midway between hematite and magnesioferrite (Fig. 8) have the largest cation deficiencies, 0.14–0.17 cations pfu (Fig. 9).

The site occupancies of the intermediate phase $(Al_{0.5}Fe^{3+}_{0.5})(MgAl_{0.5}Fe^{3+}_{0.5})O_4$, determined by Bacon and Welch (1954) suggest that substitution of Al^{3+} for Fe^{3+} takes place in both the octahedral and tetrahedral sites of the inverse spinel structure. Since $MgAl_2O_4$ is a normal spinel, a miscibility gap on the spinel-magnesioferrite join is to be expected; it may correspond to the compositional break between Sp_{100} and $Sp_{80}Mf_{20}$ (Fig. 8).

Several of the oxide masses consist of intergrowths of hematite and magnesioferrite solid solutions. The general association of the more aluminous hematites with the more aluminous magnesioferrites (Fig. 10) and their textures suggest high-temperature oxidation-driven "exsolution" analogous to that observed in the Fe-Ti oxides (Haggerty, 1976). The magnesioferrite limb of the solvus

dome appears to extend all the way to $Sp_{80}Mf_{20}$ (Fig. 10). Crystals having compositions approximately midway between Fe_2O_3 and $Fe^{3+}(Fe^{3+}Mg)O_4$ (Fig. 8) and having the greatest cation deficiency do not show any visible signs of crystalline inhomogeneity at 400× magnification.

The only Ti-rich oxide observed in this sample was a slightly Fe-deficient, Al- and Mg-bearing pseudobrookite of very limited compositional variability (Table 7). It occurs principally as rare, translucent euhedral crystals imbedded in the silicate phases. Nowhere was pseudobrookite observed in contact with other oxides. The extremely small size (approximately 1 μm × 10 μm) and lathlike habit of the crystals is probably responsible for their low analytical totals and the presence of minor Mg, Ca, and Si in their electron-microprobe analyses.

Summary and conclusions

Detailed electron-microprobe microanalysis and X-ray powder-diffraction analysis of a sample of coal-fire buchite revealed the presence of Fe^{3+}-rich clinopyroxenes, melilites, and oxides. The melilites and iron oxides have chemical compositions heretofore unreported in nature.

Clinopyroxene compositions straddle the diopside (Di)–ferri-aluminum Tschermaks (FATs) join and range from $Di_{80}FTs_{12}CaTs_8$ to $Di_9FTs_{52}CaTs_{39}$. Although a complete range of compositions on this join has been synthesized, the most Fe^{3+}-rich natural pyroxene previously reported, also from a coal-fire buchite (Cosca and Essene, 1985), had the approximate formula $Di_{15}FTs_{37}CaTs_{48}$. Cation assignments based on accepted conventions suggest a maximum substitution of 0.17 Fe^{3+} atoms pfu in the tetrahedral sites of compositions approaching endmember FATs. This represents the greatest amount of Fe^{3+} substitution reported in the tetrahedral site of a natural pyroxene.

The most unusual silicates observed in this study are the extremely Fe^{3+}- and Al-rich melilites. No melilite compositions even remotely approaching these have been reported from experimental studies or as natural samples. These compositions reflect extensive coupled substitution of the type $Fe^{3+} + Al^{3+} = Si^{4+} + R^{2+}$ away from the "gehlenite-ferrigehlenite" join, $R_2^{2+}(Al_2SiO_7)$–$R_2^{2+}(Fe_2SiO_7)$, and toward the hypothetical endmember $R^{2+}R^{3+}(R_3^{3+}O_7)$; the crystals contain 25–50 mol% of the latter endmember. Unlike the substitution of Fe^{3+} for tetrahedral Al along the gehlenite-ferrigehlenite join, concomitant substitution of Fe^{3+} and Al for Si and R^{2+} appears to involve both the four- and eight-coordinated sites in the melilite structure and results in a higher Fe^{3+} content than in endmember ferrigehlenite. The extremely high Fe^{3+} content and restricted range of compositional variation (lack of extensive substitution toward the gehlenite-ferrigehlenite join) suggest that the coal-burn melilite may not be isostructural with gehlenite.

The oxides are represented by hematite and magnesioferrite, both of which show extensive $Al^{3+} \rightarrow Fe^{3+}$ substitution. Substitution extends from magnesioferrite, $Fe^{3+}(Fe^{3+}Mg)O_4$, along the spinel-magnesioferrite join to $Sp_{80}Mf_{20}$ and along the magnesioferrite-hematite join to $Mf_{60}Hm_{40}$ with most compositions lying in the Al-rich field and characterized by a slight defect. The break in composition between $Sp_{100}Mf_0$ and $Sp_{80}Mf_{20}$ probably corresponds to the miscibility gap between the normal and the inverse (magnesioferrite) spinel structure. Microchemical analysis of the hematite-magnesioferrite intergrowths suggests the presence of a solvus dome, one limb of which extends from magnesioferrite to $Sp_{80}Mf_{20}$.

The coal-fire buchite from Buffalo, Wyoming, is extremely heterogeneous on a scale of tens to hundreds of micrometers, consisting of chemical domains within which each phase has an approximately uniform composition. Thus, while the bulk sample represents extreme disequilibrium, local equilibrium may exist within domains. The heterogeneity of this sample, despite the probability that the protolith was of uniform composition, is thought to be due to the effects of extreme and highly transient temperature gradients that resulted in partial fractional fusion and recrystallization. A detailed investigation of paragenesis and the interrelationships of phase compositions is now underway.

Inasmuch as coal burns represent an unusual and relatively unexplored natural environment of mineral formation, it is not surprising that new mineral composi-

Table 7. Electron-microprobe analyses of magnesioferrites and pseudobrookite

	Crystal 91*	Crystal 79*	Crystal 70	Pseudo-brookite**
		Weight percent		
SiO_2	0.14	0.00	0.11	1.40(62)
Al_2O_3	55.38	4.74	2.84	1.27(15)
TiO_2	0.24	0.00	0.21	33.10(35)
Fe_2O_3	21.86	73.65	86.85	58.02(67)
Cr_2O_3	0.51	0.00	0.00	0.03(1)
MnO	0.28	1.26	1.90	0.36(2)
NiO	0.07	0.00	0.12	0.01(1)
MgO	20.56	19.18	8.46	1.13(13)
CaO	0.07	0.06	0.28	1.17(29)
Na_2O	0.00	0.07	0.00	n.d.
K_2O	0.00	0.00	0.00	n.d.
Total	99.11	98.96	100.76	96.49
		Cations per four oxygens		
Si	—	—	—	0.06
Al	1.69	0.18	0.11	0.07
Ti	—	—	0.01	1.00
Fe^{3+}	0.43	1.83	2.21	1.77
Cr	0.01	—	—	—
Mn	0.01	0.04	0.05	0.01
Ni	—	—	—	—
Mg	0.79	0.94	0.43	0.07
Ca	—	—	0.01	0.05
Na	—	—	—	—

Formulas

Crystal 91: $(Al_{0.72}Fe^{3+}_{0.21}\square_{0.07})(Al_{0.97}Mg_{0.79}Fe^{3+}_{0.22}Mn_{0.01}Cr_{0.01})O_4$
Crystal 79: $(Fe^{3+}_{0.91}Al_{0.08}\square_{0.01})(Mg_{0.94}Fe^{3+}_{0.92}Al_{0.10}Mn_{0.04})O_4$
Crystal 70: $(Fe^{3+}_{2.21}Mg_{0.43}Al_{0.11}Mn_{0.05}Ti_{0.01}Ca_{0.01}\square_{0.18})O_4$
Pseudobrookite: $(Fe^{3+}_{1.77}Al_{0.07}Mg_{0.07}Si_{0.05}Ca_{0.05}Mn_{0.01})TiO_5$

* Cations in aluminous magnesioferrites assigned on the basis of (1) all Mg in six-coordination, (2) equal distribution of Fe in four- and six-coordination, and (3) all other first-transition elements in six-coordination. These assignments conform to those for $(Al_{0.5}Fe_{0.5})(MgAl_{0.5}Fe_{0.5})O_4$ reported by Bacon and Welch (1954).

** Average of several point analyses on three different crystals.

tions have been discovered. Further studies will, no doubt, reveal the existence of heretofore unexpected mineral compositions and perhaps new minerals. Thus, coal burns should provide a fertile field for future mineralogical studies.

Acknowledgments

We thank Subrata Ghose and H. G. Huckenholz for their thoughtful reviews of our manuscript.

References

Akasaka, Masahida. (1983) ^{57}Fe Mössbauer study of clinopyroxenes in the join $CaFe^{3+}AlSiO_6$-$CaTiAl_2O_6$. Physics and Chemistry of Minerals, 9, 205–211.

Akasaka, Masahida, and Onuma, Kosuke. (1980) The join $CaMgSi_2O_6$-$CaFeAlSiO_6$-$CaTiAl_2O_6$ and its bearing on the Ti-rich fassaitic pyroxenes. Contributions to Mineralogy and Petrology, 71, 301–312.

Bacon, G.E., and Welch, A.J.E. (1954) An X-ray examination of the spinel-type mixed oxide $MgFeAlO_4$. Acta Crystallographica, 7, 361–363.

Barron, V., Rendon, J.L., Torrent, J., and Cordoba, C.J. (1984) Relation of infrared, crystallochemical, and morphological properties of aluminum substituted hematites. Clays and Clay Minerals, 32, 475–479.

Bigham, J.M., Golden, D.C., Bowen, L.H., Buol, S.W., and Weed, S.B. (1978) Iron oxide mineralogy of well-drained ultisols and oxisols: 1. Characterization of iron oxides in soil clays by Mössbauer spectroscopy, X-ray diffractometry and selected chemical techniques. Journal of the American Soil Science Society, 42, 816–825.

Bowen, N.L., Schairer, J.F., and Posnjak, E. (1933) The system CaO-FeO-SiO_2. American Journal of Science, 26, 193–284.

Cawthorn, R.G., and Collerson, K.D. (1974) The recalculation of pyroxene end member parameters and the estimation of ferrous and ferri-iron content from electron microprobe analyses. American Mineralogist, 59, 1203–1208.

Cosca, M.A., and Essene, E.J. (1985) Paralava chemistry and conditions of formation, Powder River Basin, Wyoming (abs.). EOS, 66, 396.

Cosca, M.A., Peacor, D.R., and Essene, E.J. (1985) The chemistry and structure of a natural ferri-aluminum Tschermakitic pyroxene produced by pyrometamorphism. Geological Society of America Abstracts with Programs, 17, 553.

Deer, W.A., Howie, R.A., and Zussman, J. (1963) Rock-forming minerals, 1: Ortho and ring silicates. Longman, London.

——— (1978) Rock-forming minerals, 2A: Single chain silicates. Longman, London.

DeGrave, Eddy, Verbeeck, A.E., and Chambaere, D.G. (1985) Influence of small aluminum substitutions in the hematite lattice. Physics Letters A, 107A(4), 181–184.

Devine, J.D., and Sigurdsson, H. (1980) Garnet-fassaite calc-silicate nodule from La Soufrière, St. Vincent. American Mineralogist, 65, 302–305.

Dobrovolny, Ernest. (1981) Geologic map of the Buffalo quadrangle, Johnson County, Wyoming. U.S. Geological Survey Geologic Quadrangle Map GQ-1552.

Dyson, D.J., and Juckes, L.M. (1972) A silica deficient pyroxene in iron ore sinters. Mineralogical Magazine, 38, 872–877.

Fysh, S.A., and Clark, P.E. (1982) Aluminous hematite: A Mössbauer study. Physics and Chemistry of Minerals, 8, 257–267.

Ghose, Subrata, Wan, Che-ng, Okamura, F.P., and Weidner, J.R. (1975) Site preference and crystal chemistry of transition metal ions in pyroxenes and olivines (abs.). Acta Crystallographica, sec. A, 31, S76.

Ginzburg, I.V. (1969) Immiscibility of the natural pyroxenes diopside and fassaite and the criterion for it. Doklady Academy of Sciences USSR, Earth Science Section, 186, 106–109.

Haggerty, S.E. (1976) Oxidation of opaque mineral oxides in basalts. Mineralogical Society of America Reviews in Mineralogy, Hg-1–Hg-100.

Hartman, Piet. (1969) Can Ti^{4+} replace Si^{4+} in silicates? Mineralogical Magazine, 37, 366–369.

Hazen, R.M., and Finger, L.W. (1977) Crystal structure and compositional variation of Angra dos Reis fassaite. Earth and Planetary Science Letters, 35, 357–362.

Hieke, O. (1945) I giacimenti di contatto del Monte Costone (Adamello menidionale). Memoric dell'Instituto Geologico della Universita di Padova, 15, 1–46.

Hijikata, Ken-ichi. (1968) Unit-cell dimensions of the clinopyroxenes along the join $CaMgSi_2O_6$-$CaFe^{3+}AlSiO_6$. Faculty of Science Journal, Hokkaido University, Series 4, Geology and Mineralogy 4, 149–157.

Hijikata, Ken-ichi, and Onuma, Kosuke. (1969) Phase equilibria of the system $CaMgSi_2O_6$-$CaFe^{3+}AlSiO_6$ in air. Japanese Association of Mineralogists, Petrologists, and Economic Geologists Journal, 62, 209–217.

Hooper, R.L. (1982) Mineralogy of a coal burn near Kemmerer, Wyoming. M.S. thesis, Washington State University, Pullman.

Hooper, P.R., and Atkins, L. (1969) The preparation of fused samples in X-ray fluorescence analysis. Mineralogical Magazine, 37, 409–413.

Huckenholz, H.G., and Ott, W.D. (1978) Synthesis, stability, and aluminum-iron substitution in gehlenite-ferrigehlenite solid solutions. Neues Jahrbuch für Mineralogie Monatshefte, 521–536.

Huckenholz, H.G., Lindhuber, W., and Springer, J. (1974) The join $CaSiO_3$-Al_2O_3-Fe_2O_3 of the CaO-Al_2O_3-Fe_2O_3-SiO_2 quaternary system and its bearing on the formation of granditic garnets and fassaitic pyroxenes. Neues Jahrbuch für Mineralogie Abhandlungen 121, 160–207.

Huggins, F.E., Virgo, D., and Huckenholz, H.G. (1977) Titanium-containing silicate garnets. 1. The distribution of Al, Fe^{3+}, Ti^{4+} between octahedral and tetrahedral sites. American Mineralogist, 62, 475–490.

Kimata, M., and Ii, N. (1981) The crystal structure of synthetic akermanite, $Ca_2MgSi_2O_7$. Neues Jahrbuch für Mineralogie Monatshefte, H.I., 1–10.

——— (1982) The structural property of synthetic gehlenite, $Ca_2Al_2SiO_7$. Neues Jahrbuch für Mineralogie Abhandlungen, 144, 254–267.

Knopf, Adolph, and Lee, D.E. (1957) Fassaite from near Helena, Montana. American Mineralogist, 42, 73–77.

Kurepin, V.A., Polshin, E.V., and Alibekov, G.I. (1981) Intracrystalline distribution of iron (3+) and aluminum cations in clinopyroxene ($CaFe^{3+}AlSiO_6$). Mineralogicheskii Zhurnal, 3, 83–88.

Louisnathan, S.J. (1971) Refinement of the crystal structure of a natural gehlenite, $Ca_2Al(Al,Si)_2O_7$. Canadian Mineralogist, 10, 822–837.

Majmundar, H.H. (1971) Fassaite from Madagascar. Canadian Mineralogist, 10, 899–903.

Mapel, W.J. (1959) Geology and coal resources of the Buffalo–Lake DeSmet area, Johnson and Sheridan Counties, Wyoming. U.S. Geological Survey Bulletin 1078, 148 p.

Mason, Brian. (1974) Aluminum-titanium-rich pyroxenes with special reference to the Allende meteorite. American Mineralogist, 59, 1198–1202.

Muan, Arnulf, and Gee, C.L. (1956) Phase equilibrium studies in the system iron oxide–γ-Al_2O_3 in air at 1 atm O_2 pressure. American Ceramic Society Journal, 39, 207–214.

Nurse, R.W., and Midgley, H.G. (1953) Studies in the melilite solid solutions. Iron and Steel Institute Journal, 174, 121–131.

Ohashi, Haruo, and Hariya, Yu. (1973) Order-disorder of ferric iron and aluminum in the system $CaMgSi_2O_6$-$CaFeAlSiO_6$ at high pressure. Japanese Association Mineralogists, Petrologists, and Economic Geologists Journal, 68, 230–233.

Osborn, E.F., and Schairer, J.F. (1941) The ternary system pseu-

dowollastonite-åkermanite-gehlenite. American Journal of Science, 239, 715–763.
Peacor, D.R. (1967) Refinement of the crystal structure of a pyroxene of formula $M_1M_{11}(Si_{1.5}Al_{0.5})O_6$. American Mineralogist, 52, 31–41.
Rao, A.T., and Rao, M.V. (1970) Fassaite from a calc-silicate skarn vein near Gondivalosa, Orissa, India. American Mineralogist, 55, 975–980.
Schwertmann, U., Fitzpatrick, R.W., and Le Roux, J. (1977) Al substitution and differential disorder in soil hematites. Clays and Clay Minerals, 25, 373–374.
Schwertmann, U., Fitzpatrick, R.W., Taylor, R.M., and Lewis, D.G. (1979) The influence of Al on iron oxides. Part II. Preparation and properties of Al-substituted hematites. Clays and Clay Minerals, 27, 105–112.
Seifert, F. (1974) The join åkermanite-ferroåkermanite. Carnegie Institution of Washington Year Book 73, 436–440.
Solymar, Karoly, and Jonas, Klara. (1971) A goethite racsaba beepult Al-tartalom vizsgalata is jelentosege a magyar bauxitokban. Kohasz Lapok, 104, 226–235.
Tilley, C.E. (1938) Aluminous pyroxenes in metamorphosed limestones. Geological Magazine, 75, 81–86.
Tomasi, L. (1940) Fassaite di val di solda e sua paragenesi. Studi Trentini di Scienze Naturali, 21, 85–111.
von Steinwehr, H.E. (1967) Gitterkonstanten im system α-$(Al,Fe,Cr)_2O_3$ und ihr Abweichen von der Vegardregal. Zeitschrift für Kristallographie Mineralogie, 125, 377–403.
Willemse, J., and Bensch, J.J. (1964) Inclusions of original carbonate rocks in gabbro and norite of the eastern part of the Bushveld complex. Geological Society of South Africa Transactions, 67, 1–87.
Yoder, H.S. (1950) Stability relations of grossularite. Journal of Geology, 58, 221–253.

Manuscript received January 2, 1986
Manuscript accepted September 2, 1986